Available online at www.sciencedirect.com

ScienceDirect

Journal of Ocean Engineering and Science 1 (2016) 238–245

www.elsevier.com/locate/joes

Numerical study on cavitating flow due to a hydrofoil near a free surface

Ping-Chen Wu [a], Jiahn-Horng Chen [b,*]

[a] Department of Naval Architecture and Ocean Engineering, Osaka University, Osaka, Japan
[b] Department of Systems Engineering and Naval Architecture, National Taiwan Ocean University, Keelung, Taibei, China

Received 15 December 2015; accepted 26 February 2016
Available online 8 April 2016

Abstract

A numerical strategy is proposed for a viscous uniform flow past a 2-D partially cavitating hydrofoil placed at a finite depth from the free surface. The flow was modeled by the Reynolds-averaged Navier–Stokes (RANS) equations. A finite-volume method with the SIMPLE scheme and k-ε turbulence model were employed for computations. The "full cavitation model," which included the effects of vaporization, noncondensible gases and compressibility, was incorporated in the computation of cavitating flow. The cavity shape and free surface were updated iteratively till a reasonable convergence was reached. As for the determination of the free surface, the VOF approach was adopted. The test cases show the accuracy and stability of our procedure to capture the cavitating flow near the free surface.

Keywords: Cavitation; Viscous flow; Free surface; 2-D hydrofoil; Two-phase flow.

1. Introduction

Due to its complicated physics, cavitation has been an interesting and challenging flow problem for scientists and engineers. Phenomena involved in cavitation are usually highly nonlinear, unsteady, transient, multi-phase, mixing, and phase changing. Furthermore, in many practical applications, the device or vehicle which may induce cavitation operates within a finite water depth. The effects due to the free surface are usually not negligible. This fact makes the physics even more complicated and the analysis more time-consuming when the computational approach is taken in the study.

The pioneering study of cavitation near the free surface is primarily within the linear and inviscid scope. The conformal mapping technique is the main solution procedure. Due to its inherent mathematical properties, such an approach is restricted to two-dimensional problems. Applying the linearized cavitating flow theory developed for an infinite depth, Johnson [10] pioneered the design of supercavitating hydrofoils operating at a finite depth and zero cavitation number. Meanwhile, Auslaender [1] employed the linearized cavity flow theory and a mapping technique to study general characteristics of two-dimensional supercavitating or fully ventilated hydrofoils for operation near a free surface.

Later, the development of lifting-line and lifting-surface theories enables one to extend the study to three-dimensional linearized problems. Nishiyama and Miyamoto [16] used a lifting-surface theory to take into account the three-dimensional effects. Nishiyama [15] provided another solution procedure based on the lifting line method. Both of them are fully linearized theories and only applicable to the flow at small angles of attack and small cavitation numbers. In addition, they did not consider the effects due to the thicknesses of the body and the cavity.

With the progress of the theoretical development, the non-linear theories soon dominate the study of the cavitating flow near the free surface. Larock and Street [12] employed the conformal mapping approach to calculate the supercavitating flat-plate hydrofoil. Later, Furuya [6] developed an iterative procedure to investigate the two-dimensional gravity-free flow past supercavitating hydrofoils. The thickness effects of the body and/or the cavity were taken into account. The results were more accurate, compared to those

* Corresponding author.
E-mail address: jhcntou@gmail.com (J.-H. Chen).

http://dx.doi.org/10.1016/j.joes.2016.02.002

obtained by the linearized theory. In addition, Furuya [7] investigated the three-dimensional flow past a supercavitating hydrofoil of large aspect ratio. He treated the flow near the foil as two-dimensional and introduced a three-dimensional correction based on Prandtl's lifting-line theory. It should be pointed out that the above-mentioned works were limited to the condition of infinite Froude number (zero gravity). A few years later, Doctors [4] linearized the free-surface condition for finite Froude numbers. He studied the flow past a two-dimensional supercavitating, arbitrarily-shaped hydrofoil by distributing Kelvin-type sources and vortices along the mean line of foil and cavity. His results show that the effect of the Froude number is more important when the cavity length is greater.

The advance of modern computers brings in rapid development of computational methods. The boundary element method (BEM) became an important tool in the study of the inviscid cavitating flow near the free surface which has been widely investigated theoretically. Through the computational approach, the shape of the cavity and body can be easily taken into consideration. Therefore, the cavitating flow can be more accurately predicted by using proper cavitation models. In addition, three dimensional effects can also be readily explored. Lee et al. [13] first pioneered such an approach to solve two-dimensional flows past partially and supercavitating hydrofoils under a free surface. Later, Young and Kinnas [21] developed a nonlinear BEM for surface-piercing propeller. The study which could trace cavity shape and free surface was carried out by Bal et al. [2].

Recently, the rapid development of computational fluid dynamics has made it possible to take into account the effects of viscosity and turbulence. Such progress makes the simulation more realistic. Furthermore, more complicated and practical cavitation models can be incorporated in the approach. Kubota et al. [11] first introduced a two-phase flow cavity model which could explain the interaction between viscous effects. More recently, Senocak and Shyy [18] conducted a systematic overview of numerical simulations of viscous cavitating flows based on the solution of Navier–Stokes equations. Singhal et al. [19] proposed a "full cavitation model," which took several factors related to the phase change into consideration. They include the formation and transport of vapor bubbles, the turbulent fluctuations of pressure and velocity, and the magnitude of noncondensible gases. In addition to the Reynolds-averaged Navier–Stokes equations (RANS), they also solved the Rayleigh–Plesset equations to simulate the detail of bubble dynamics. It is evident that the simulation of cavitating flow becomes more and more complicated.

However, it is quite unfortunate that all these studies have not yet included effects due to the free surface. In fact, the studies available in the literature seldom investigate viscous cavitation near a free surface. It is not until recently that study of this issue has been conducted. Jin et al. [9] carried out a numerical study on ventilated cavitating flow near a free surface with a cavitation model developed by Merkle et al. [14]. They focused on the ventilated cavitation process. Brizzolara and Young [3] investigated the physical and theoretical modeling of surface-piercing hydrofoils. They employed a volume-of-fluid technique with a mixture flow model in computations for both foil-born and take-off conditions.

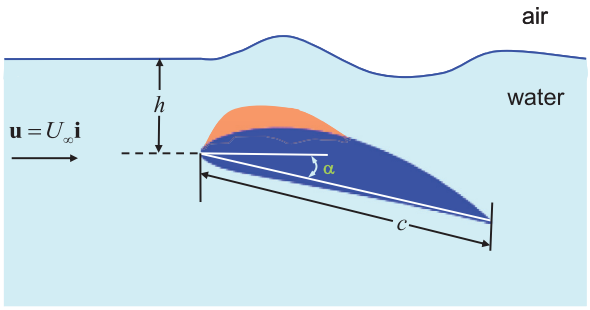

Fig. 1. The cavitating flow near the free surface.

The purpose of the present study is to develop a numerical procedure to compute such a flow with complicated physical phenomena. Our approach employs the full cavitation model to simulate the cavitating flow and a volume of fluid (VOF) method [8] to capture the free surface. Although both of them are based on the concept of volume of fraction, they have to be treated separately. This is due to the fact that the former must satisfy the Rayleigh–Plesset equations but the latter need not. An iteration procedure was developed to update iteratively the free surface and the cavity surface. We focus on the 2-D partial cavitating hydrofoil at a finite depth from the free surface. The flow field was governed by RANS (Reynolds-averaged Navier–Stokes equations) and solved by finite-volume method with SIMPLE algorithm. The turbulence model is k-ε turbulence model.

2. Theoretical formulation and numerical procedure formatting

Shown in Fig. 1, a uniform viscous flow with free surface passes around a two-dimensional hydrofoil with a chord length c. The far-upstream incoming velocity is U_∞ in the x-direction. The angle of attack is α. The depth from the free surface of calm water to the leading edge of the hydrofoil is h. Partial cavitation takes place on the upper surface of the hydrofoil and waves are generated on the free surface when the fluid passes around it.

The equations governing the cavitation phenomena can be expressed by

$$\frac{\partial \rho_m}{\partial t} + \nabla \cdot (\rho_m \mathbf{u}_m) = \dot{m}, \tag{1}$$

$$\frac{\partial}{\partial t}(\rho_m \mathbf{u}_m) + \nabla \cdot (\rho_m \mathbf{u}_m \mathbf{u}_m) = \rho_m \mathbf{g} - \nabla p + \nabla \cdot \left[\mu_m (\nabla \mathbf{u}_m + \nabla \mathbf{u}_m^T)\right] + \nabla \cdot \left[\sum_{k=1}^{2} \alpha_k \rho_k \mathbf{u}_{dr,k} \mathbf{u}_{dr,k}\right]. \tag{2}$$

The symbols are defined as follows. First of all, the index m represents "mixture;" ρ_m is the density of liquid-gas mixture fluid defined as

$$\rho_m = \sum_{k=1}^{2} \alpha_k \rho_k, \tag{3}$$

where α_k and ρ_k denote the volume fraction and the fluid density of phase k, respectively. For convenience, we let $k=1$ represent the liquid phase and $k=2$ the gas phase (vapor). The symbol $\mathbf{u}_m$ represents the velocity of mixture fluid,

$$\mathbf{u}_m = \frac{\sum_{k=1}^{2} \alpha_k \rho_k \mathbf{u}_k}{\rho_m}, \tag{4}$$

$\dot{m}$ is the phase-changing mass rate; $\mathbf{g}$ is the gravity; p is the pressure field; μ_m is the dynamic viscosity of the mixture fluid,

$$\mu_m = \sum_{k=1}^{2} \alpha_k \mu_k. \tag{5}$$

In addition, $\mathbf{u}_{dr,k}$ represents the drift velocity,

$$\mathbf{u}_{dr,k} = \mathbf{u}_k - \mathbf{u}_m. \tag{6}$$

It should be noted that, if the effects due to non-condensable gases are taken into account, Eq. (3) should be modified as

$$\rho_m = \sum_{k=1}^{2} \alpha_k \rho_k + (1-\alpha_1-\alpha_2)\rho_n, \tag{7}$$

where ρ_n represents the density of non-condensable gases for which the volume fraction is $(1-\alpha_1-\alpha_2)$.

For the turbulence model, we employed the k–ε model. In a cavitating flow field, the equations for k and ε can be expressed as

$$\begin{aligned}
&\frac{\partial}{\partial t}(\rho_m k) + \nabla\cdot(\rho_m \mathbf{u}_m k) = \nabla\cdot\left(\frac{\mu_{t,m}}{\sigma_k}\nabla k\right) + G_{k,m} - \rho_m \varepsilon,\\
&\frac{\partial}{\partial t}(\rho_m \varepsilon) + \nabla\cdot(\rho_m \mathbf{u}_m \varepsilon) = \nabla\cdot\left(\frac{\mu_{t,m}}{\sigma_k}\nabla \varepsilon\right) + \frac{\varepsilon}{k}\\
&\qquad\qquad \times (C_{1\varepsilon} G_{k,m} - C_{2\varepsilon}\rho_m \varepsilon),
\end{aligned} \tag{8}$$

where

$$\begin{aligned}
&\mu_{t,m} = \rho_m C_\mu \frac{k^2}{\varepsilon},\\
&G_{k,m} = \mu_{t,m}\left[\nabla \mathbf{u}_m + (\nabla \mathbf{u}_m)^T\right] : \nabla \mathbf{u}_m.
\end{aligned} \tag{9}$$

The constants shown in the above two equations are similarly defined as those for the single-phase flow.

For the cavitation model, the "full cavitation model" proposed by Sinhal et al. [19] was employed. To simplify the study, we assume that (1) the fluid in liquid phase is incompressible and the fluid in gas phase is compressible and (2) the temperature effects are negligible. Under these assumptions, the mass fraction of gas phase, f, satisfies

$$\frac{\partial}{\partial t}(\rho_m f) + \nabla\cdot(\rho_m \mathbf{u}_2 f) = \nabla(\gamma \nabla f) + R_e - R_c, \tag{10}$$

where γ represents the effective phase exchange coefficient; R_e and R_c are the source terms denoting evaporation and condensation rates, respectively. These two source terms can be derived from the Rayleigh–Plesset equations and are given by

$$R_e = C_e \frac{V_{ch}}{\sigma}\rho_1 \rho_2 (1-f)\sqrt{\frac{2(p_v - p)}{3\rho_1}} \quad \text{for } p < p_v, \tag{11}$$

and

$$R_c = C_c \frac{V_{ch}}{\sigma}\rho_1 \rho_2 f\sqrt{\frac{2(p - p_v)}{3\rho_1}} \quad \text{for } p > p_v, \tag{12}$$

where C_e and C_c are empirical constants which are 0.02 and 0.01, respectively; V_{ch} is the characteristic velocity; σ is the surface tension of liquid; p_v the phase-change threshold pressure. Suggested by Sinhal et al. [19], turbulence effects can have significant influence on cavitation. Therefore, the threshold pressure p_v includes the turbulent pressure fluctuations and is estimated by

$$p_v = \frac{1}{2}(p_{sat} + p_{turb}), \tag{13}$$

where p_{sat} is the liquid saturation vapor pressure and p_{turb} is given by

$$p_{turb} = 0.39\rho_m k. \tag{14}$$

To treat the two-phase flow due to the presence of the free surface, we employed the volume-of-fluid method which is applicable when the gas and liquid cannot be exchanged. Let β_k denote the volume fraction of phase k, then the mass conservation law requires

$$\frac{\partial \beta_k}{\partial t} + \mathbf{u}\cdot\nabla\beta_k = 0. \tag{15}$$

Of course, the volume fraction should satisfy the additional condition

$$\sum_{k=1}^{2} \beta_k = 1. \tag{16}$$

Finally, in the present study, we have three non-dimensional parameters

$$\text{Reynolds number: } Re = \frac{\rho U_\infty c}{\mu}, \tag{17}$$

$$Froude\ number: Fn = \frac{U_\infty}{\sqrt{gc}}, \tag{18}$$

$$Cavitation\ number: \sigma = \frac{p_{op} + \rho g h - p_{sat}}{\frac{1}{2}\rho U_\infty^2}. \tag{19}$$

In our study, the finite volume method was employed to discretize the governing equations. The discretization procedure is a standard one. The solution method is based on the SIMPLE algorithm developed by Patankar and Spalding [17]. The algorithm corrects the velocity and pressure fields iteratively. In addition, the first-order upwind scheme was employed for the interpolations of vapor, turbulence kinetic energy (k) and dissipation rate (ε), the second-order upwind scheme for momentum, and the body-force weighted scheme for pressure.

In the flow computations, there two kinds of gas phase: the air above the free surface and the vapor due to evaporation of water in cavitation. Even though they are of one kind in terms of their phase, they have to be treated separately due to different physical considerations. The air above the free surface is incompressible and non-exchangeable with the liquid phase; the vapor, on the contrary, is compressible and can be

exchanged to or from the liquid phase in the condensation or evaporation process. To cope with these differences in computations, we devise an iterative procedure to compute the cavitating flow and to capture the free surface. The iterative steps are described as follows.

(a) Assuming the hydrofoil is fully wetted, we first compute the flow field without cavitation and capture the free surface by using the VOF method. We assume the free surface coincides with the contour line where the volume fraction β_1 takes the value of 0.5.
(b) The mesh is regenerated according to the free surface obtained in step (a). The new mesh excludes the area occupied by the air above the free surface.
(c) Fixing the shape of the free surface, we then compute the cavitating flow around the hydrofoil by using the full cavitation model. Here, the velocity distribution on the free surface and the static pressure distribution on the outlet boundary are specified as parts of boundary conditions. Again, we assume the cavity surface coincides with the contour line where the volume fraction α_1 takes the value of 0.5.
(d) The mesh is regenerated according to the surface of the cavity obtained in step (c). The new mesh includes the area occupied by the air and excludes the areas occupied by the cavity and the hydrofoil.
(e) Fixing the cavity shape, we again compute the flow field and update the free surface by using the VOF method. Here, the "mean" tangential velocity distribution on the cavity surface is specified as the boundary conditions on it.
(f) Repeat the steps (b) to (e) till a proper convergence of the cavity shape and free surface is achieved.

There are several criteria we specified in steps (a), (c) and (e) to ensure a proper convergence. First of all, the residuals of continuity equation, the velocity components and the volume fraction must be less than some tolerance ε_1. In addition, in steps (a) and (e), the mean variation of the free surface shape must be less than the required tolerance ε_2 during iterations. And, in step (c), the change of the lift coefficient and the mean variation of the cavity shape have to be less than another required tolerances ε_3 and ε_4 during iterations, respectively.

3. Test cases

We first briefly describe the computational domain and the mesh used for computations. The infinite domain must be properly truncated before the mesh can be generated and computations follow. In our study, the upstream and downstream boundaries are set at $5c$ from the leading edge and $10c$ from the trailing edge, respectively. The mesh was then generated by the commercial code GRIDGEN. We divided the computational domain into two areas. For the area around the hydrofoil, which is smaller, we employed an unstructured fine grid in order to capture the cavity shape accurately. For the other part somewhat far away from the hydrofoil, an H-type of grid was generated. The mesh in this part is relatively coarse, compared to the unstructured one. Nevertheless, the H-grid is nearly orthogonal so that we can capture the free surface with a higher accuracy. In the present iterative strategy, re-gridding is required in every iteration to capture the free and cavity surfaces. A typical grid after several iterations is shown in Fig. 2.

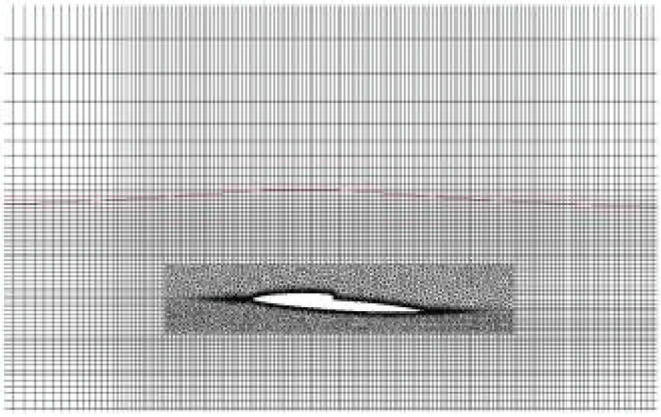

Fig. 2. Typical grid after several iterations.

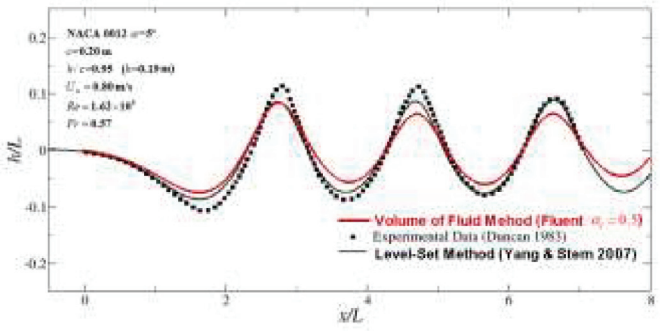

Fig. 3. The wave due to the uniform flow past a non-cavitating hydrofoil.

For the following computations, the water temperature was specified to be 25 °C. At this condition, the saturation pressure of water, p_{sat}, is 3,540 Pa, the water density 998.2 kg/m^3, and its vapor density 0.5542 kg/m^3. In addition, water and vapor viscosity are 1.003×10^{-3} kg/m-s and 1.34×10^{-5} kg/m-s, respectively. The air viscosity is 1.789×10^{-5} kg/m-s and air density 1.225 kg/m^3. Furthermore, the gravity acceleration is 9.81 m/s^2, and the mass fraction of the non-condensable gas in the water is 1.5×10^{-5}.

To proceed to computation of the cavitating flow near the free surface, we first conducted two tests. The first one is the flow past a fully wetted hydrofoil near the free surface. This is to verify the capability of capturing the free surface. A NACA 0012 hydrofoil was employed for the test. The angle of attack of the incoming flow is 5 degrees. The other parameters are set at $h/c=0.951$, $Re=1.624\times10^5$, and $Fn=0.5672$. Fig. 3 shows the wave form of the present result at $\beta_1=0.5$ and its comparison to the experimental data by Duncan [5] and the simulation results of Yang and Stern

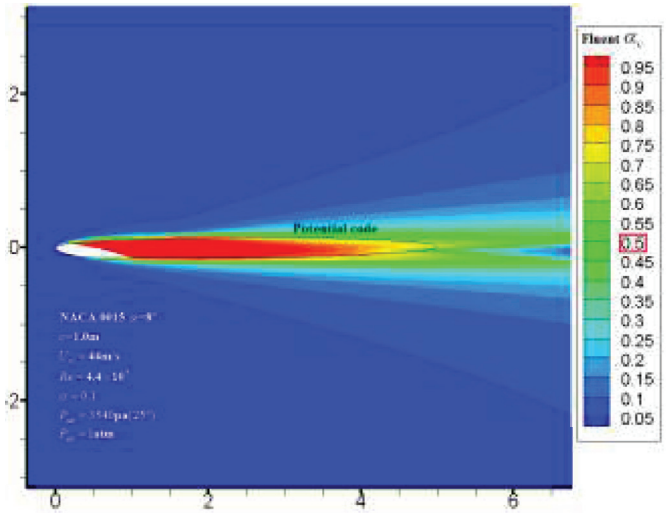

Fig. 4. The vapor distribution for flow past a cavitating hydrofoil (without free surface).

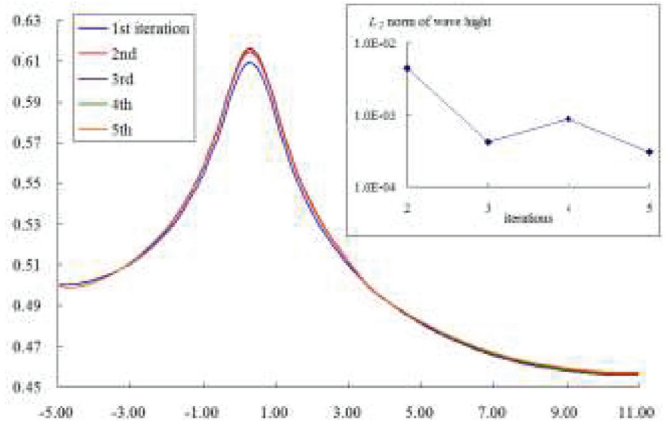

Fig. 5. The convergence history of the free surface at $\sigma = 1.0$.

[20]. It is evident that the wave trend and frequency are close to each other, but the amplitude of the present study is somewhat smaller and decays somewhat faster. This may be due to the dissipative nature of VOF method and the effects of the somewhat coarse grid distribution near the free surface and away from the flow field. A better result can be obtained if a finer grid is employed. Nevertheless, this test confirms that we can capture the free surface. In addition, according to the result, we specify the contour line at $\beta_1 = 0.5$ to be the water surface which separates the water from the air in computing the cavitating flow.

The second test is the cavitating flow over a hydrofoil without the free surface. This is to verify the capability of capturing the cavitation and cavity. A NACA 0015 hydrofoil was employed for test. The angle of attack of the free stream is 8 degrees. Other parameters are set at $Re = 4.4 \times 10^7$, and $\sigma = 0.1$. Fig. 4 shows the distribution of the vapor fraction. We compare the result with that obtained by the potential flow model. It appears that the contour line of $\alpha_1 = 0.5$ is well-consistent with the cavity shape obtained by potential

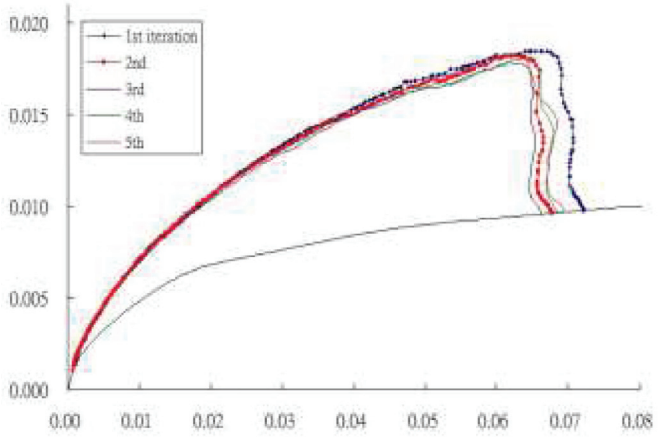

Fig. 6. The convergence history of the cavity surface at $\sigma = 1.0$.

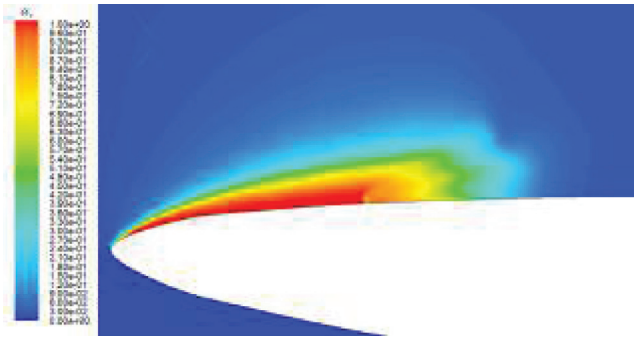

Fig. 7. The vapor fraction distribution around the hydrofoil at $\sigma = 1.0$.

code. Therefore, in the following computations, we specify the contour line at $\alpha_1 = 0.5$ to be the cavity surface which separates the vapor from the water in computing the cavity surface.

We proceed to the computations of the cavitating flow near the free surface. In the present study, the section of the hydrofoil is NACA 16-006. The angle of attack is 4 degrees. The non-dimensional depth of the hydrofoil at the leading edge $h/c = 0.5$. Two different cavitation numbers were employed.

For the first case, the cavitation number $\sigma = 1.0$. Correspondingly, we have the incoming speed $U_\infty = 14.3$ m/s, the Reynolds number $Re = 1.433 \times 10^7$ and the Froude number $Fn = 4.89$. Fig. 5 shows the convergence history of the free surface. In five iterations of VOF computation, the free surface is well convergent. In fact, after the third iteration, the variation of the free surface is within the range of negligence. The convergence history of the cavity shape is shown in Fig. 6. It is obvious that the same convergence conclusion can be drawn. That is, after the third iteration, the variation is not significant except in the region of bubble closure. The convergent results show that the hydrofoil is partially cavitating at the leading edge and the cavity length is about $0.07c$. The cavity is small. The maximum wave height is 0.114 m appearing at the location almost directly above the leading edge of the hydrofoil. Its magnitude implies that the free surface effect is not negligible.

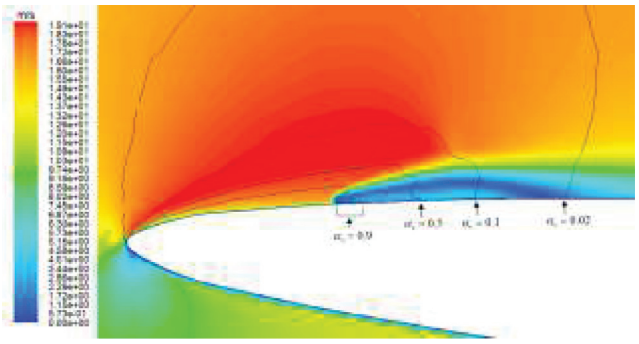

(a) Velocity contour.

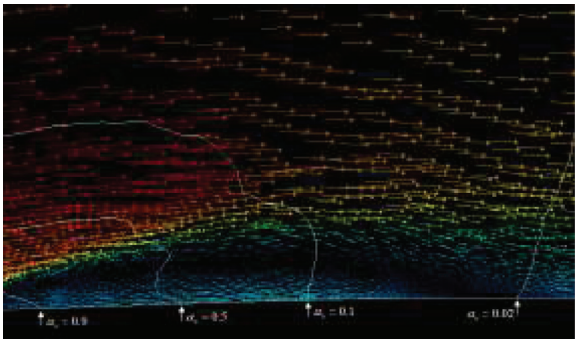

(b) Velocity vectors.

Fig. 8. The velocity field near the region where the cavitation occur at $\sigma = 1.0$.

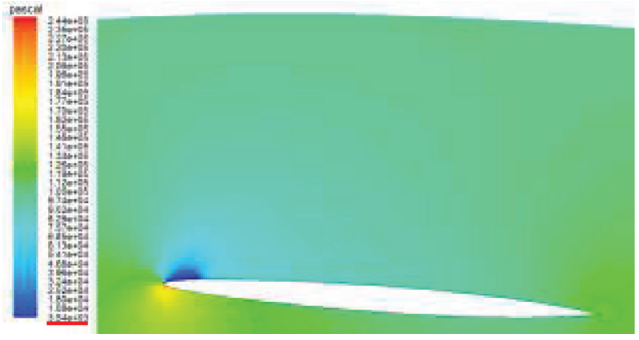

(a) Distribution of static pressure.

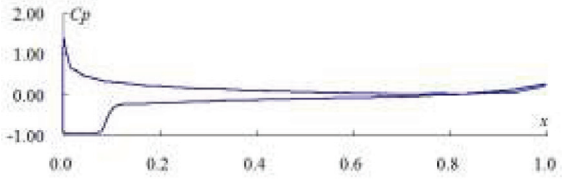

(b) c_p on the hydrofoil surface.

Fig. 9. Pressure distributions at $\sigma = 1.0$.

Fig. 7 shows the vapor fraction distribution in the region near the cavitating area. Fig. 8 shows the velocity field near the region where the cavitation occurs. Observing these two plots, it is interesting to find that right after the pure vapor region where only vapor occupies ($\alpha_v = 1.0$), a low-speed

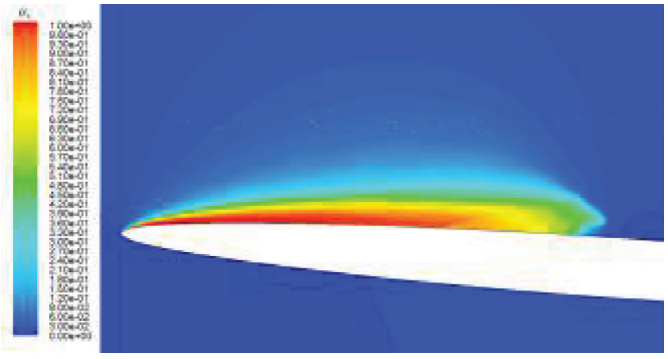

Fig. 10. The vapor fraction distribution around the hydrofoil at $\sigma = 0.5$.

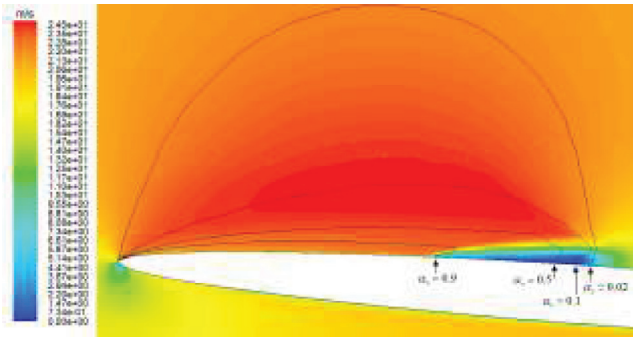

(a) Velocity contour.

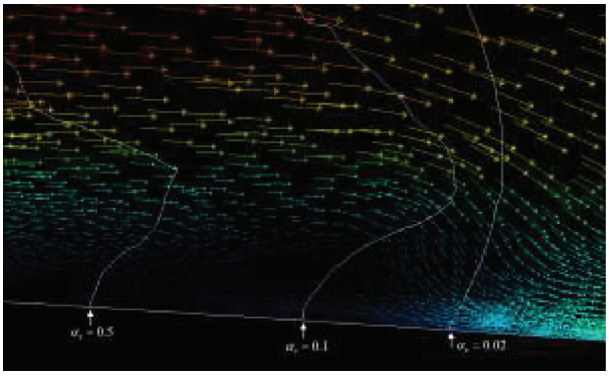

(b) Velocity vectors.

Fig. 11. The velocity field near the region where the cavitation occur at $\sigma = 0.5$.

recirculating region follows. This region grows downstream. The flow re-attaches the hydrofoil surface at a point where the vapor fraction is very small ($\alpha_v \approx 0.02$). It appears that the flow in the cavity closure region is quite chaotic. This phenomenon was also observed in the results without the free surface by Senocak and Shyy [18].

The pressure field and its coefficient distribution on the hydrofoil surface is shown in Fig. 9. On the surface where the cavitation occurs, the pressure coefficient keeps a constant value which corresponds to the value of p_{sat}. Basically, the high-speed region has a lower pressure distribution and vice versa. Furthermore, the static pressure increases gradually in

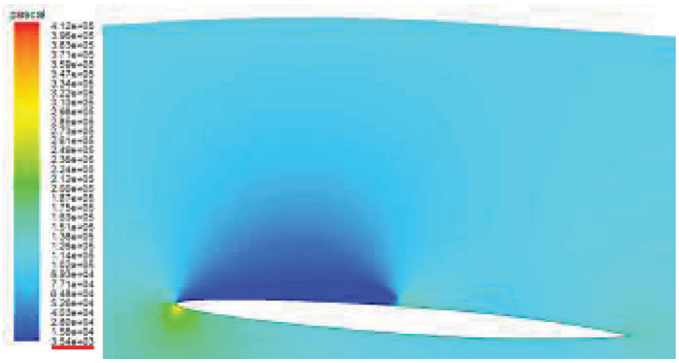

(a) Distribution of static pressure.

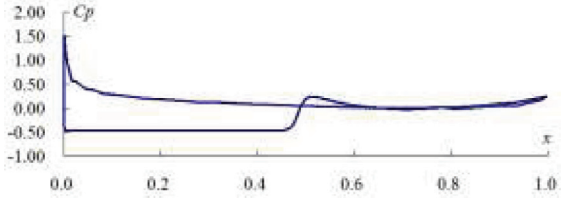

(b) c_p on the hydrofoil surface.

Fig. 12. Pressure distributions at $\sigma = 0.5$.

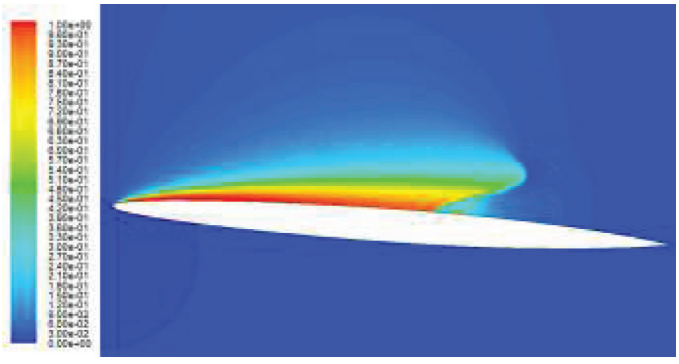

Fig. 13. The vapor fraction distribution without a free surface at $\sigma = 0.5$.

the vertical direction due to the hydrostatic pressure induced by gravity.

In the second test, the cavitation number $\sigma = 0.5$. The corresponding incoming velocity is 20.3 m/s and the Froude number is 6.47. The convergence history is similar to that in the first case. Within five iterations, the iterative computation achieved its convergence within the specified tolerance criteria. The maximum wave height is about 0.135 m, only 0.02 m higher than that in the first case. Nevertheless, the cavitation bubble is much longer. The vapor fraction and velocity distributions are shown in Figs. 10 and 11. The contour with $\alpha_v = 0.5$ represents the cavity surface. The cavity is about $0.45c$ in length. Again, there exists a low-speed recirculating region right after the pure vapor region. Similarly, the region re-attaches the hydrofoil surface at a small vapor fraction of about 0.02. The pressure distribution in the flow field and the pressure coefficient on the hydrofoil surface are shown in Fig. 12. Finally, we also computed flow at the same condition but without a free surface. The cavity surface is shown in Fig. 13. Obviously, the cavity is longer than that under a free surface. This is due to that the wave peak appears just above the leading edge area and results in a higher static pressure.

4. Conclusions

In the present work, an iterative numerical procedure to combine fully cavitation model and the VOF method has been developed for a cavitating hydrofoil near a free surface. A convergent solution can be properly achieved within several iterations. Therefore, through the present iterative procedure, we can capture the cavitating flow near the free surface. The test cases show that convergence in the computation of the free surface is quite good in the use of the VOF method. Nevertheless, the convergence in the computation of the cavity shape is somewhat slower. This is especially true in the region of the bubble tail or cavity closure.

Acknowledgments

The present study was made possible by the financial support of National Science Council of the Republic of China under the Grant NSC 95-2221-E-019-090. The authors would like to express their thanks to this support.

References

[1] J. Auslaender, J. Ship Res. 6 (1962) 8–23.
[2] S. Bal, S.A. Kinnas, H. Lee, J. Ship Res. 45 (2001) 34–49.
[3] S. Brizzolara, Y.L. Young, in: Proceedings of the 31st International Conference on Ocean, Offshore and Arctic Engineering, ASME, Rio de Janeiro, Brazil, 2012.
[4] L.J. Doctors, J. Ship Res. 30 (1986) 1–11.
[5] J.H. Duncan, J. Fluid Mech. 126 (1983) 507–520.
[6] O. Furuya, J. Fluid Mech. 68 (1975) 21–44.
[7] O. Furuya, J. Fluid Mech. 71 (1975) 339–359.
[8] C.W. Hirt, B.D. Nichols, J. Comput. Phys. 39 (1981) 201–225.
[9] M.S. Jin, C.T. Ha, W.G. Park, J. Mech. Sci. Technol. 27 (12) (2013) 3683–3691.
[10] V.E. Johnson, Theoretical and Experimental Investigation of Supercavitating Hydrofoils Operating near the Free Water Surface Technical Report, TR R93, NASA, 1961.
[11] A Kubota, H Kato, H. Yamaguchi, J. Fluid Mech. 240 (1992) 59–96.
[12] B.E. Larock, R.L. Street, J. Fluid Mech. 29 (1967) 317–336.
[13] C.S. Lee, J.M. Lew, Y.G. Kim, in: Proceedings of the 19th Symposium on Naval Hydrodynamics, Korea, 1992, pp. 605–618.
[14] C.L. Merkle, D. Li, S. Venkateswaran, in: Proceedings of the 42th Joint Propulsion Conference Exhibit, AIAA, Sacramento, CA, 2006.
[15] T. Nishiyama, Z. Angew. Math. Mech. 50 (1970) 645–653.
[16] T. Nishiyama, M. Miyamoto, Lifting-Surface Method for Calculating the Hydrodynamic Characteristics of Supercavitating Hydrofoil Operating near the Free Water Surface, 34 Technical Report, Tohoku University, 1969, pp. 123–139.
[17] S.V. Patankar, D.B. Spalding, Int. J. Heat Mass Transf. 15 (1972) 1787–1806.

[18] I. Senocak, W. Shyy, in: Proceedings of the 4th International Symposium on Cavitation, Pasadena, CA, 2001.
[19] A.K. Singhal, M.M. Athavale, H. Li, Y. Jiang, J. Fluids Eng. 124 (2002) 617–624.
[20] J. Yang, F. Stern, in: Proceedings of the 45th AIAA Aerospace Sciences Meeting Exhibit, Reno, NV, 2007.
[21] Y.L. Young, S.A. Kinnas, in: Proceedings of the 4th International Symposium on Cavitation, Pasadena, CA, 2001.